Computational Mechanics manuscript No.
(will be inserted by the editor)

Isogeometric blended shells for dynamic analysis: simulating aircraft takeoff and the resulting fatigue damage on the horizontal stabilizer

Ning Liu · Manoj R. Rajanna · Emily L. Johnson · Jim Lua · Nam Phan · Ming-Chen Hsu

Abstract Aircraft horizontal stabilizers are prone to fatigue damage induced by the flow separation from aircraft wings and the subsequent impingement on the stabilizer structure in its wake, which is known as a buffet event. In this work, the previously developed isogeometric blended shell approach is reformulated in a dynamic analysis setting for the simulation of aircraft takeoff using varying pitch angles. The proposed Kirchhoff–Love (KL) and continuum shell blending allows the critical structural components of the aircraft horizontal stabilizer to be modeled using continuum shells to obtain high-fidelity 3D stresses, whereas the less critical components are modeled using computationally efficient KL thin shells. The imposed aerodynamic loads are generated from a hybrid immersogeometric and boundary-fitted computational fluid dynamics (CFD) analysis to accurately record the dynamic excitation on the stabilizer external surface. Specifically, the entire aircraft except for the wings and stabilizers is immersed into a non-boundary-fitted fluid domain based on the immersogeometric analysis (IMGA) concept for computational savings, whereas the mesh surrounding the aircraft wing and stabilizers is boundary-fitted to accurately compute the aerodynamic loads on the stabilizer. The obtained time histories of the loads are then applied to dynamic blended shell analysis of the horizontal stabilizer, and the high-fidelity stress response is evaluated for subsequent fatigue assessment. A simple frequency-domain fatigue analysis is then carried out to evaluate the buffet-induced fatigue damage of the stabilizer. The results from both the steady-state and dynamic nonlinear blended shell analyses of a representative horizontal stabilizer demonstrate the numerical accuracy and computational efficiency of the proposed approach.

Keywords isogeometric analysis · Kirchhoff–Love shell · continuum shell · buffet–induced fatigue damage · aircraft takeoff simulation

N. Liu (✉) · J. Lua
Global Engineering & Materials, Inc., Princeton, NJ 08540, USA
E-mail: nliu@gem-innovation.com

M.R. Rajanna · M.-C. Hsu
Department of Mechanical Engineering, Iowa State University, Ames, IA 50011, USA

E.L. Johnson
Department of Aerospace and Mechanical Engineering, University of Notre Dame, Notre Dame, IN 46556, USA

N. Phan
Structures Division, Naval Air Systems Command (NAVAIR), Patuxent River, MD 20670, USA

1 Introduction

Aircraft horizontal stabilizers are vulnerable to fatigue failure caused by the flow separation from aircraft wings and the subsequent impingement on the stabilizer structure in its wake, which is known as a buffet event. In the computational community, one of the traditional approaches to model such an event is to perform boundary-fitted computational fluid dynamics (CFD) analysis to obtain the time histories of the aerodynamic loads, followed by structural analysis of the stabilizer to obtain stress results for fatigue evaluation. In terms of the structural analysis, solid or solid-like shell elements in standard finite element (FE) methods are frequently employed in order to get accurate 3D stress predictions for multiaxial fatigue evaluation [1, 2]. However, they are typically very computationally expensive. In cases where thin shell elements (e.g., Kirchhoff–Love (KL) shells [3, 4]) are employed, the transverse stress and strain components cannot be accurately obtained. On the CFD analysis side, in order to obtain high-fidelity CFD loads on the structure, three prerequisites are needed: (a) a watertight geometry for analysis-suitable mesh generation, (b) a boundary-fitted mesh to accurately approximate the geometry, and (c) a proper numerical projection technique to map the CFD loads to the structure. This results in several challenges. For

one thing, the geometry cleanup process often consumes the majority of the design-to-analysis time and significant manual effort to obtain a satisfactory geometry to start with. For another, data loss is sometimes unavoidable during the projection process for the CFD loads.

In order to bypass the time-consuming geometry cleanup process and avoid the approximation error that arises from the FE mesh generation, the concept of isogeometric analysis (IGA) [5] has gained significant attention in the past decade and become a widely used method especially for the simulation of structures comprised of complicated geometries [6–16]. A notable benefit of using the IGA-based description is that the underlying computational model is geometrically exact and is described by high-order basis functions, which allows faster solution convergence with fewer elements [17–19]. In the analysis of shell-like structures, a large variety of IGA shell formulations of the KL type [3, 4, 20, 21] and the continuum type [22–26] has been developed. Moreover, efficient coupling formulations for multi-patch analysis [27–30] have been presented to realize direct analysis on multi-patch NURBS models. These approaches have also been recently extended to a blended shell formulation [31, 32] that allows patch coupling between various shell types. From the perspective of dynamic analysis, IGA shells have been applied across a wide range of applications, including wind turbine blades [33–40] and heart valves [12, 41–48].

In this context, we propose to extend the previously developed isogeometric blended shell approach [31] to the dynamic analysis setting to analyze the effects of time-dependent buffet loads acting on the aircraft horizontal stabilizer. The proposed formulation is applicable to both non-conforming and non-smooth patch interfaces in the coupling of isogeometric shells of different types. In the modeling of the aircraft horizontal stabilizer for dynamic analysis, the use of the blended shell approach allows us to deploy continuum shell elements only at critical locations to accurately predict the 3D stress information and incorporate KL thin shells in less critical regions to improve the computational efficiency. On the other hand, to facilitate realistic aerodynamic load generation, an FE-based, hybrid immersogeometric [49] and boundary-fitted analysis (IMGA-BF) approach is adopted to obtain the CFD loads during the takeoff simulation. The FE-based compressible flow simulations using only boundary-fitted mesh has been successfully applied to simulate full-scale aircraft aerodynamics problems [50, 51]. Given that aircraft components (e.g., fuselage and engine) are often geometrically complex and their corresponding CAD models are "dirty" in the sense that the constituting B-rep surfaces are usually either non-watertight or overlapped with each other, the use of immersogeometric analysis (IMGA) [42, 49, 52–56] bypasses the geometry cleanup process and does not require a boundary-fitted mesh for analysis, which significantly improves the analysis flexibility. For components that require high solution accuracy in terms of flow or load prediction, the standard boundary-fitted approach is adopted. This hybrid approach allows the solution to be both computationally efficient and numerically accurate. The use of finite elements for fluids and IGA for shells also allows us to transfer the load through L^2- projection of the traction and globally conserves forces and moments acting on the structure [34].

After the time histories of the high-fidelity 3D stresses are obtained from the dynamic blended shell analysis, a simple frequency-domain fatigue analysis is carried out to assess the buffet-induced fatigue damage and structural integrity of the stabilizer. While time-domain fatigue methods are generally considered more accurate and can handle arbitrary loading sequences, they are relatively computationally expensive and are not well suited for large amounts of data characterized by high frequencies, as is the case in buffet-induced structural vibration. On the contrary, frequency-domain methods characterize the structural response using power spectral density (PSD) functions and are able to provide a fast evaluation of the resulting fatigue damage on the structure. Furthermore, as opposed to the time-domain methods that essentially describe the structural response as a function of time, the frequency-domain counterparts provide additional valuable insight about the characteristics of the structure such as the frequency range related to a buffet event, which is meaningful in the design viewpoint. In the present study, the equivalent von Mises stress method [57] is adopted to convert the multiaxial stress states into a uniaxial stress for quick fatigue assessment. While a multiaxial fatigue damage model is more appropriate to process the 3D stress data, it is out of the scope of the current study and the use of the simple frequency-domain fatigue analysis is merely intended to demonstrate the complete workflow of the computational framework.

This paper is structured as follows. In Section 2, the extension of the isogeometric blended shell approach for dynamic analysis is presented. A brief discussion on the adopted hybrid IMGA-BF approach for CFD analysis and the Arbitrary Lagrangian–Eulerian (ALE) framework for pitching aircraft simulation is also given. The developed blended shell formulation is then applied in Section 3 to dynamic analysis of a representative horizontal stabilizer to demonstrate the numerical accuracy and efficiency of the method, followed by a dynamic analysis and fatigue evaluation of the stabilizer subjected to a series of realistic aerodynamic loads generated from the aircraft takeoff simulation. Finally, in Section 4, conclusions about the proposed method are drawn.

2 The proposed approach

The proposed modeling approach consists of two parts, one being the extension of the isogeometric blended shell approach [31] to compute the dynamic structural response for fatigue evaluation, and the other being the use of a hybrid IMGA-BF approach for variable angle of attack CFD analysis to obtain high-fidelity structural loads. This work focuses more on the former to efficiently model the aircraft stabilizer and obtain 3D stress results without compromising computational efficiency, while the latter is briefly discussed.

2.1 Isogeometric blended shell formulation

In the proposed structural description, an isogeometric blended shell approach is utilized to couple isogeometric shells of different types though a penalty-based formulation. This penalty formulation enforces the displacement and rotational continuities in a variational manner and is applicable to non-conforming and non-smooth interfaces. The involved isogeometric shell formulations consist of a KL shell type [4, 27] for efficient computation of non-critical structures and a continuum shell type [22] to obtain high-fidelity 3D stress responses of critical structures. The formulation is briefly introduced in the following, with more details available in Liu et al. [31].

The variational formulation of the isogeometric continuum shell can be expressed through the principle of virtual work, where the contribution of the body force is neglected for brevity:

$$\delta W = \delta W^{\text{int}} - \delta W^{\text{ext}} = \int_{\Omega_0} \delta\mathbf{E} : \mathbf{S}\,\mathrm{d}\Omega - \int_{\Gamma_0^{\text{h}}} \delta\mathbf{u}\cdot\mathbf{h}\,\mathrm{d}\Gamma = 0\,, \quad (1)$$

where W is the total work, W^{int} is the internal work, W^{ext} is the external work, δ indicates the variation with respect to the virtual displacement variable $\delta\mathbf{u}$, $\mathbf{S}$ is the second Piola–Kirchhoff stress tensor, $\mathbf{E}$ is the Green–Lagrange strain tensor, Ω_0 is the shell volume in the undeformed configuration, $\mathbf{h}$ is the surface traction, and Γ_0^{h} is the undeformed boundary where $\mathbf{h}$ is applied.

Without loss of generality, let patch Ω^{A} be a continuum shell patch and patch Ω^{B} be a KL shell patch (see Figure 1). These patches are connected at an interface $\mathcal{L}$, which is chosen to be the midsurface edge of the KL shell body. The goal of the formulation is to provide both displacement and rotational continuities across the interface $\mathcal{L}$. Specifically, we augment the principle of virtual work by the penalty contribution:

$$\delta W = \delta W^{\text{int}} + \delta W^{\text{pd}} + \delta W^{\text{pr}} - \delta W^{\text{ext}} = 0\,, \quad (2)$$

where δW^{pd} and δW^{pr} are the displacement and rotational penalty contributions, respectively. The coupling conditions are enforced across the entire interface through an integration over the thickness domain $\mathcal{T}$ in order to properly constrain the interfacial continuum shell kinematics. Specifically, the displacement continuity is enforced by penalizing the relative motion of displacements at the corresponding through-thickness locations of Ω^{A} and Ω^{B} as follows,

$$\delta W^{\text{pd}} = \int_{\mathcal{L}}\int_{\mathcal{T}} \alpha_{\text{d}} \left(\mathbf{u}^{\text{A}} - \mathbf{u}^{\text{B}}\right)\cdot\left(\delta\mathbf{u}^{\text{A}} - \delta\mathbf{u}^{\text{B}}\right)\mathrm{d}\mathcal{T}\,\mathrm{d}\mathcal{L}\,, \quad (3)$$

with $\mathbf{u}^{\text{A}}$ and $\mathbf{u}^{\text{B}}$ the displacements at the corresponding through-thickness locations on Ω^{A} and Ω^{B}, respectively, and α_{d} the displacement penalty parameter. Moreover, the rotational continuity can be imposed by expanding the rotational penalty work δW^{pr} as:

$$\begin{aligned}\delta W^{\text{pr}} = &\int_{\mathcal{L}}\int_{\mathcal{T}} \alpha_{\text{r}} \Big(\left(\mathbf{g}_3^{\text{A}}\cdot\mathbf{a}_3^{\text{B}} - \mathring{\mathbf{g}}_3^{\text{A}}\cdot\mathring{\mathbf{a}}_3^{\text{B}}\right)\left(\delta\mathbf{g}_3^{\text{A}}\cdot\mathbf{a}_3^{\text{B}} + \mathbf{g}_3^{\text{A}}\cdot\delta\mathbf{a}_3^{\text{B}}\right)\\ &+ \left(\mathbf{g}_n^{\text{A}}\cdot\mathbf{a}_3^{\text{B}} - \mathring{\mathbf{g}}_n^{\text{A}}\cdot\mathring{\mathbf{a}}_3^{\text{B}}\right)\left(\delta\mathbf{g}_n^{\text{A}}\cdot\mathbf{a}_3^{\text{B}} + \mathbf{g}_n^{\text{A}}\cdot\delta\mathbf{a}_3^{\text{B}}\right)\Big)\mathrm{d}\mathcal{T}\,\mathrm{d}\mathcal{L}\,,\end{aligned} \quad (4)$$

with $\mathbf{a}_3^{\text{B}}$ the unit vector normal to the KL shell reference surface, $\mathbf{g}_3^{\text{A}}$ the surface normal of the continuum shell, $\mathbf{g}_n^{\text{A}}$ the in-plane covariant unit vector normal to the penalty plane $\mathcal{L}\times\mathcal{T}$, as illustrated in Figure 1, and α_{r} the rotational penalty parameter. Geometric variables indicated by $\mathring{(\cdot)}$ refer to the undeformed configuration.

Taking variations of δW with respect to the discrete nodal displacements and adding the contribution of the dynamic problem, Eq. (2) becomes,

$$\mathbf{R} = \mathbf{M}\ddot{\mathbf{u}} + \mathbf{C}_{\text{d}}\dot{\mathbf{u}} + \mathbf{F}^{\text{int}} - \mathbf{F}^{\text{ext}} + \mathbf{F}^{\text{pd}} + \mathbf{F}^{\text{pr}} = \mathbf{0}\,, \quad (5)$$

with $\mathbf{R}$ being the residual vector and $\mathbf{F}^{\text{int}}$, $\mathbf{F}^{\text{ext}}$, $\mathbf{F}^{\text{pd}}$, and $\mathbf{F}^{\text{pr}}$ denoting the internal, external, displacement, and rotational penalty forces, respectively. The first two terms on the right-hand side of the first equality sign in Eq. (5) account for the dynamic contributions, where $\mathbf{M}$ is the mass matrix, $\ddot{\mathbf{u}}$ is the acceleration, $\mathbf{C}_{\text{d}}$ is the damping matrix, and $\dot{\mathbf{u}}$ is the velocity.

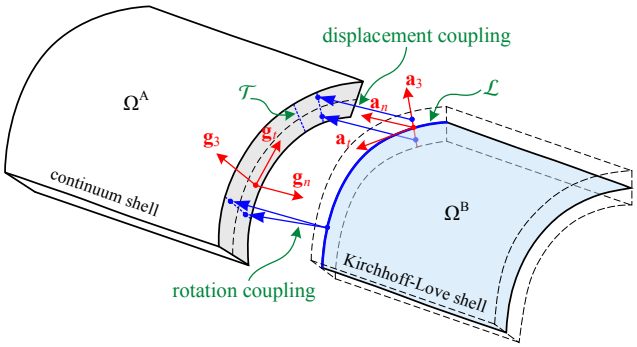

Fig. 1: An illustration of the blended coupling interface between a continuum shell and a KL shell.

For dynamic simulations, the generalized-α method [58–60] is adopted for time integration. Specifically, the solution field at a given time instance can be obtained by interpolation between the two neighboring time steps t_n and t_{n+1} as follows,

$$\mathbf{u}_\alpha = \alpha_f \mathbf{u}_{n+1} + (1-\alpha_f)\mathbf{u}_n \,, \tag{6}$$

$$\dot{\mathbf{u}}_\alpha = \alpha_f \dot{\mathbf{u}}_{n+1} + (1-\alpha_f)\dot{\mathbf{u}}_n \,, \tag{7}$$

$$\ddot{\mathbf{u}}_\alpha = \alpha_m \ddot{\mathbf{u}}_{n+1} + (1-\alpha_m)\ddot{\mathbf{u}}_n \,, \tag{8}$$

where α_f and α_m are interpolation factors, and the subscript α denotes interpolated variables. The displacement and velocity fields at the time step t_{n+1} can be calculated based on the Newmark update in the following,

$$\mathbf{u}_{n+1} = \mathbf{u}_n + \Delta t \dot{\mathbf{u}}_n + \frac{1}{2}(\Delta t)^2 \left((1-2\beta)\ddot{\mathbf{u}}_n + 2\beta \ddot{\mathbf{u}}_{n+1}\right) \,, \tag{9}$$

$$\dot{\mathbf{u}}_{n+1} = \dot{\mathbf{u}}_n + \Delta t \left((1-\gamma)\ddot{\mathbf{u}}_n + \gamma \ddot{\mathbf{u}}_{n+1}\right) \,, \tag{10}$$

where β and γ are the Newmark parameters and Δt is the time increment (i.e. $\Delta t = t_{n+1} - t_n$).

Accordingly, the residual force vector in Eq. (5) is rewritten using the α-level interpolated variables and solved for the acceleration field using:

$$\frac{\mathrm{d}\mathbf{R}_\alpha}{\mathrm{d}\ddot{\mathbf{u}}_{n+1}} \Delta \ddot{\mathbf{u}}_{n+1} = -\mathbf{R}_\alpha \,. \tag{11}$$

Assuming a linear damping model with a constant viscous damping matrix $\mathbf{C}_\mathrm{d}$, Eq. (11) is further expanded as,

$$\begin{aligned} &\left(\alpha_m \mathbf{M} + \alpha_f \gamma \Delta t \mathbf{C}_\mathrm{d} + \alpha_f \beta (\Delta t)^2 \mathbf{K}(\mathbf{u}_\alpha)\right) \Delta \ddot{\mathbf{u}}_{n+1} \\ &\quad = -\mathbf{M}\ddot{\mathbf{u}}_\alpha - \mathbf{C}_\mathrm{d}\dot{\mathbf{u}}_\alpha - \mathbf{F}^\mathrm{int}_\alpha + \mathbf{F}^\mathrm{ext}_\alpha - \mathbf{F}^\mathrm{pd}_\alpha - \mathbf{F}^\mathrm{pr}_\alpha \,, \end{aligned} \tag{12}$$

with the interpolation factors and Newmark parameters determined with improved numerical dissipation,

$$\begin{aligned} &\alpha_m = \frac{2-\rho_\infty}{1+\rho_\infty} \,, \quad \alpha_f = \frac{1}{1+\rho_\infty} \,, \\ &\beta = \frac{(1-\alpha_f+\alpha_m)^2}{4} \,, \quad \gamma = \frac{1}{2} - \alpha_f + \alpha_m \,, \end{aligned} \tag{13}$$

where ρ_∞ is the numerical dissipation parameter that falls in the range of $[0, 1]$, and $\rho_\infty = 0.5$ is employed in the current study. Readers are referred to Kiendl et al. [4] for more detailed explanation of the generalized-α linearization approach applied to shell problems.

With regards to the determination of the penalty parameters α_d and α_r, traditional penalty approaches suffer from the problem-specific empirical selection of the penalty parameter: the enforced constraints cannot be sufficiently satisfied in the case of a relatively low penalty parameter, and the system becomes ill-conditioned if the penalty parameter is too large. This work incorporates a single and universal selection of the penalty parameter α that can be applied to both the displacement and rotational continuity imposition independent of the problem definition. The penalty parameter [31] takes the material properties, the elemental in-plane dimensions, and the shell thickness into consideration and can be expressed in the following form

$$\alpha_\mathrm{d} = \alpha \frac{E}{h\,(1-\nu^2)} \,, \quad \alpha_\mathrm{r} = \alpha \frac{E\,t_h^2}{12\,h\,(1-\nu^2)} \,, \tag{14}$$

where E is the Young's modulus, ν is the Poisson's ratio, t_h is the shell thickness, and h is the element size parameter determined by averaging the corresponding element sizes on the two patches in the direction of the penalty curve $\mathcal{L}$.

2.2 Hybrid immersogeometric and boundary-fitted CFD analysis

A hybrid IMGA-BF computational framework [49] based on stabilized finite element methods for compressible flows [61–66] is used in the current work to accurately predict the buffet loads on the horizontal stabilizer of the aircraft. The stabilized finite element method has been thoroughly validated for simulating aircraft aerodynamics problems [65, 66]. The recently proposed IMGA approach [49] directly makes use of a B-rep CAD model by immersing it into a fluid mesh and can therefore handle different geometric configurations (e.g., pylons and stores) without geometry cleanup and remeshing. However, it can be challenging to obtain high solution accuracy if the mesh is not sufficiently refined. On the other hand, the traditional boundary-fitted approach adds boundary layers surrounding the structure, which is more labor-intensive but provides higher accuracy. In order to obtain a good balance between computational efficiency and solution accuracy, we combine the two approaches to construct a unified hybrid IMGA-BF framework to accurately predict aircraft buffet loads on the stabilizer for dynamic simulation. The IMGA approach is used for non-critical parts of the aircraft to avoid time-consuming geometry cleanup, and the boundary-fitted approach is applied to critical structural components to ensure the high quality of the flow solution (cf. Figure 2). This combination achieves the maximum level of modeling efficiency, solution accuracy, and geometric flexibility, and we can effectively and accurately capture the turbulent flow generation and separation as well as the vortex shedding that impinges on the stabilizer structures. Note that this hybrid IMGA-BF framework can also handle moving domain problems using the ALE approach [49, 61], and the mixed ALE/IMGA computation falls under the concept of the Fluid–Solid Interface-Tracking/Interface-Capturing Technique (FSITICT) [67], which is the fluid–structure interaction (FSI) version of the Mixed Interface-Tracking/Interface-Capturing Technique (MITICT) [68].

Following this idea, the B-rep CAD model of the aircraft components (fuselage, engine, etc.) except for the wing and

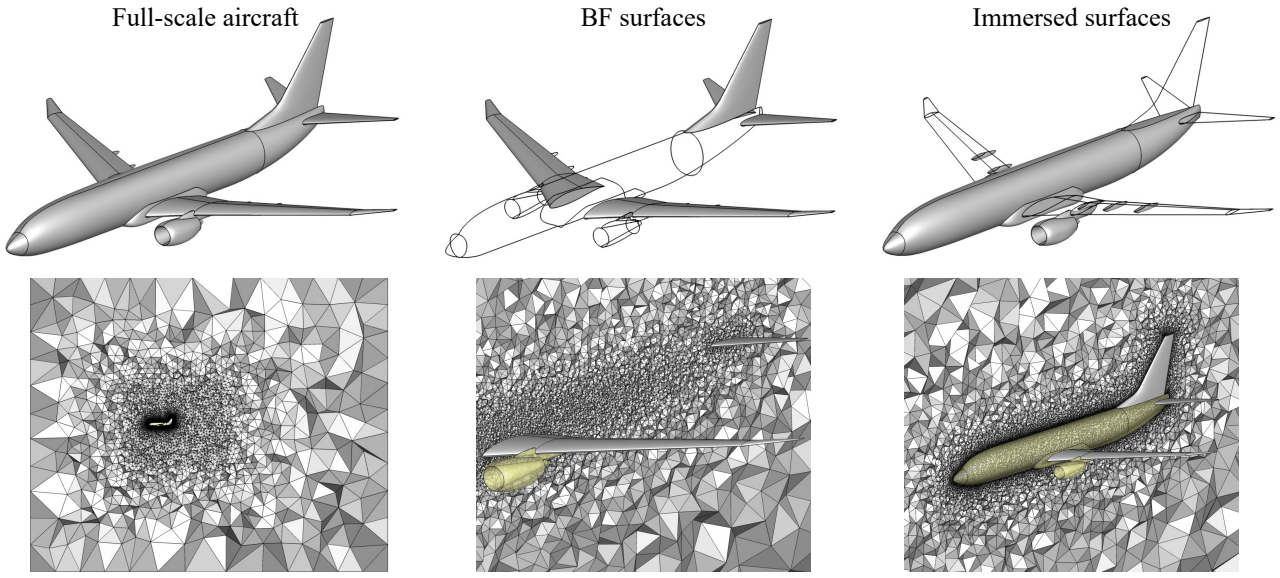

Fig. 2: The hybrid IMGA-BF surfaces and mesh of the full-scale aircraft for CFD analysis: boundary-fitted mesh around the aircraft wing and horizontal stabilizers, and IMGA mesh for the fuselage.

stabilizer are directly immersed into a non-boundary-fitted mesh of the background fluid domain, whereas a boundary-fitted mesh is generated at the aircraft wings and horizontal stabilizers to accurately capture the flow separation and its impingement on the stabilizer structure. Subsequently, an aircraft takeoff CFD simulation is carried out using time-dependent pitch angle data to record the aerodynamic loads on the external surface of the stabilizer for dynamic structural analysis and high-fidelity 3D stress prediction. The traction loads are transferred at the fluid–structure interface from the fluid discretization to the integration points of the structural discretization through L^2-projection, which globally conserves forces and moments acting on the structure.

3 Numerical results

In this section, the developed isogeometric blended shell formulation is applied to model the dynamic response of a representative horizontal stabilizer. The accuracy of the dynamic blended shells is first verified by comparing the dynamic steady-state solution of the stabilizer under a constant uniform traction load with the solutions obtained from a set of static analysis conditions using Abaqus and an isogeometric pure KL shell model [31]. The applicability of the developed blended shells is further demonstrated via sequential CFD-structural analysis, where the time-dependent aerodynamic loads acting on the horizontal stabilizer are obtained from a hybrid IMGA-BF CFD analysis of the entire aircraft and subsequently applied to the stabilizer for dynamic structural analysis. A simple frequency-domain fatigue analysis is then carried out based on the obtained time histories of the 3D stresses to demonstrate the full workflow of the simulation framework.

3.1 Validation studies of the dynamic blended shell formulation

The developed isogeometric blended shell formulation is applied to perform both static and dynamic nonlinear analysis of a representative horizontal stabilizer with internal structures, as illustrated in Figure 3, where the highlighted patch is modeled using continuum shells and the rest of the patches are modeled using KL shells. The stabilizer has root and tip chord lengths of 3.19 m and 0.7 m, respectively, and a tail semi-span of 6.75 m. The model is comprised of 6 skin patches, 10 rib patches, and 5 spar patches, modeled using bicubic NURBS with a total of 71 penalty curves for coupling. An isotropic aluminium material model is employed with E = 71.7 GPa and ν = 0.33. The thickness of

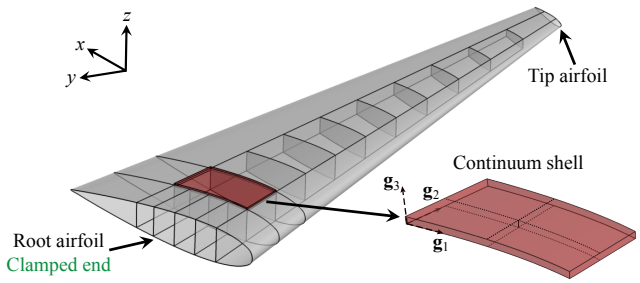

Fig. 3: A schematic of the horizontal stabilizer geometry used in analysis. The highlighted patch is modeled using isogeometric continuum shells and the rest of the patches are modeled using isogeometric KL shells.

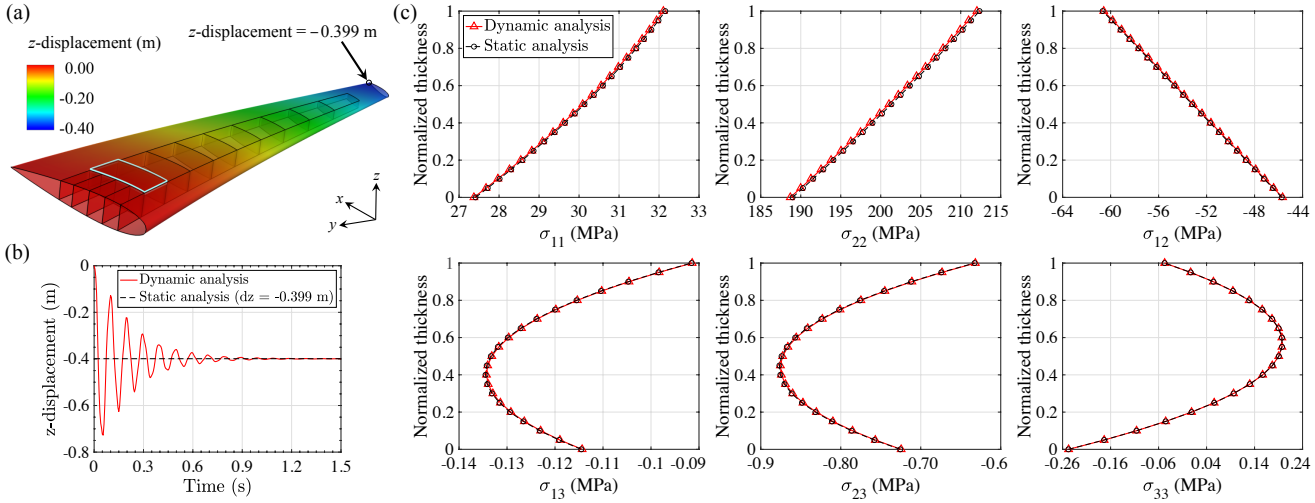

Fig. 4: Steady-state results of the dynamic blended shell analysis: (a) Displacement field contour plot for blended shell model. (b) Time history of the tip displacement compared with the static analysis result. (c) The through-thickness Cauchy stress comparison at the center of the continuum shell patch compared with the static analysis result [31].

Table 1: Solution accuracy and efficiency comparison between the Abaqus reference solution, the pure KL shell model (denoted as KL), and the proposed blended shell model (denoted as BL).

Method	Number of elements	Number of DOFs	Converged z-displacement (m)
Abaqus S4	44,410	261,720	−0.401
KL	13,744	50,331	−0.399
BL (Static)	13,744	52,761	−0.399
BL (Dynamic)	13,744	52,761	−0.399

the skin, ribs, and spars are assumed to be 0.04 m, 0.01 m, and 0.01m, respectively. The penalty parameter value of $\alpha = 10^3$ is used, as it has been determined via a variety of shell benchmark problems [27, 31] that this value holds well over a wide range of engineering applications. A uniform downward traction of 100 kPa is applied to the stabilizer skin with the root section clamped. To obtain a steady-state solution using dynamic analysis, a damping coefficient of $C_d = 1000$ kg/(m^{2}s) is applied for the entire stabilizer. This value ensures that the stabilizer reaches the steady state within a reasonable amount of time. A time step size of 1×10^{-3} is used in this simulation.

The obtained dynamic blended shell analysis results are compared against the static analysis results from an Abaqus model constructed using S4 shell elements as well as a pure isogeometric KL shell model. The deformed configuration of the stabilizer at steady state is shown in Figure 4a. The time history of the tip displacement is plotted in Figure 4b and compared with the static analysis displacement results. After the solution reaches steady state, the dynamic analysis results reach a good agreement with the static analysis results. The number of elements and the number of degrees of freedom (DOFs) required for all the simulations are listed in Table 1. Based on the obtained results, it is obvious that the developed blended shell approach is computationally efficient compared to the Abaqus model, in that only less than 20% the number of DOFs required by Abaqus for convergence is needed to achieve the same level of accuracy. Another important takeaway is that the use of the continuum shell patch does not compromise computational efficiency when utilized in the context of the blended shell approach, as is observed by the same number of elements and the relatively close number of DOFs required for convergence in the blended shell and the pure KL shell models.

The through-thickness stresses at the center of the continuum shell patch are extracted and displayed in Figure 4c for capability demonstration. As seen from the results, both the in-plane and out-of-plane components of the Cauchy stresses from dynamic analysis match very well with the static results, which further verifies the numerical accuracy of the dynamic blended shell approach. The ability to compute the full-scale Cauchy stress tensor at critical locations offers the possibility for accurate multiaxial fatigue assessment [1, 2] without compromising solution efficiency.

3.2 Aircraft takeoff simulation, dynamic analysis, and fatigue evaluation

Now that the developed isogeometric blended shell formulation is numerically verified, it is further applied to study the dynamic response of the stabilizer subjected to simulated CFD loads. An aircraft takeoff simulation using the hybrid IMGA-BF CFD analysis is performed to obtain realistic aerodynamic loads on the stabilizer surface, which is subsequently applied to the blended shell stabilizer model and the full 3D stresses at locations of interest are com-

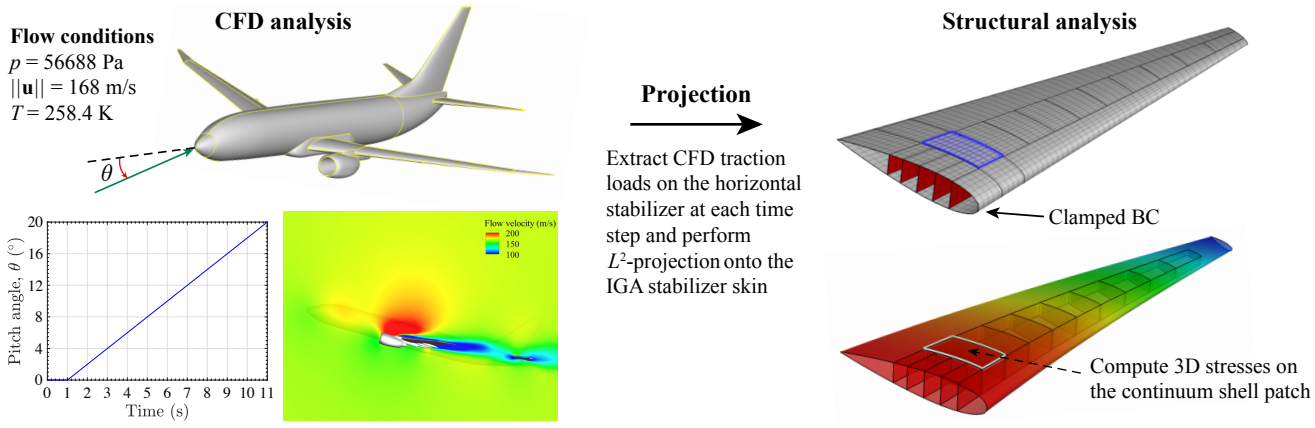

Fig. 5: The overall framework to perform dynamic analysis of the horizontal stabilizer: CFD simulation setup, exchange of CFD load data, and structural simulation setup.

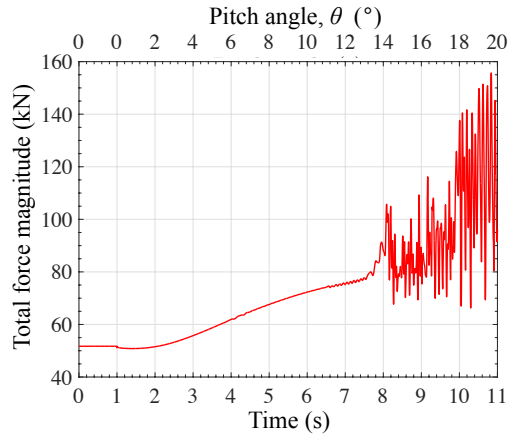

Fig. 6: Time history of the total force magnitude acting on the left horizontal stabilizer obtained using the CFD simulation.

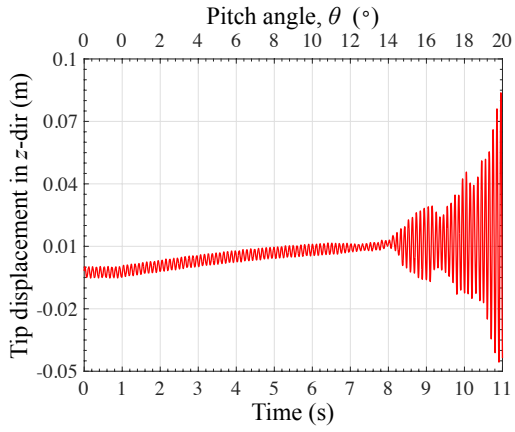

Fig. 7: Time history of the horizontal stabilizer tip displacement plot in the z-direction.

puted for fatigue evaluation. To perform the CFD simulation, we assume conditions where the aircraft is cruising at a certain speed and perform a pitch or sudden takeoff maneuvering. In this case, an inflow velocity of 168 m/s, pressure of 56,688 Pa, and temperature of 258.4 K are applied at the far-field boundaries of the computational domain. To perform the takeoff simulation, we pitch the entire fluid domain at the rate of two degrees per second and handle the moving domain problem using the ALE approach. An illustration of the hybrid mesh used in the present simulation can be found in Figure 2, and the overall computational framework is demonstrated in Figure 5, which also shows the CFD analysis setup, flow conditions, and the time history of the aircraft pitch angle. The hybrid IMGA-BF computational mesh is comprised of 14,383,139 linear tetrahedral elements. For the boundary-fitted surfaces, the size of the first element in the wall-normal direction is 0.01 m, and 10 layers of boundary-layer elements are generated with a growth ratio of 1.2. The fluid element size near the immersed surface is 0.05 m. Note that only the CFD traction loads on the left horizontal stabilizer of the aircraft are extracted and projected onto the IGA skin surface to study the dynamic responses of the blended shell structure. The same material properties as described in Section 3.1 are adopted, and the damping effects due to air are assumed to be negligible.

Figure 6 shows the total fluid force magnitude acting on the left horizontal stabilizer of the aircraft. The corresponding time history of the tip displacements of the stabilizer under the fluid traction load obtained using structural simulation is plotted in Figure 7. The results clearly demonstrate the severity of the wake of the unsteady flow hitting the stabilizer at higher aircraft pitch angles. Under the dynamic CFD loads, the horizontal stabilizer vibrates severely at higher pitch angles, and the amplitude of the vibration increases with increasing aircraft pitch angle. To illustrate the flow behavior, Figure 8 shows the fluid velocity contour along the midplane of the horizontal stabilizer, and Figure 9 shows the contour plot of the fluid traction magnitude acting on the horizontal stabilizer at different time instances and pitch angles. Figure 10 shows the deformation of the stabilizer overlapped with the reference configuration at various

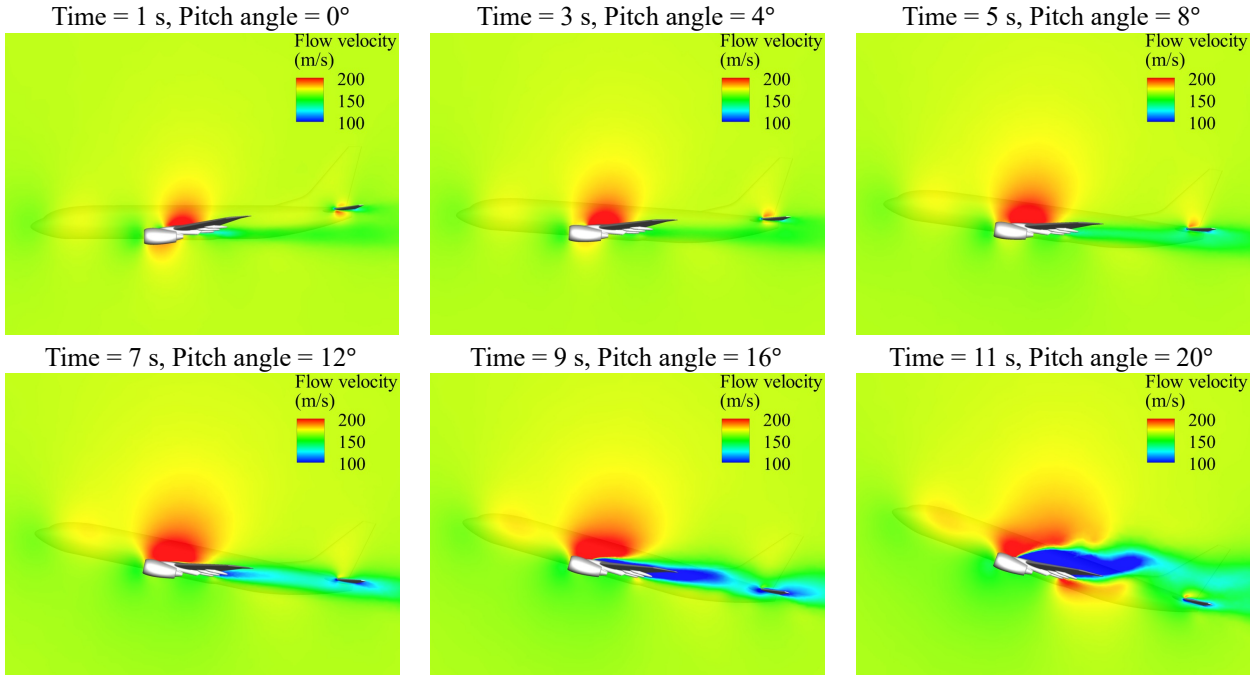

Fig. 8: Fluid flow contour along the midplane of the horizontal stabilizer at different time instances.

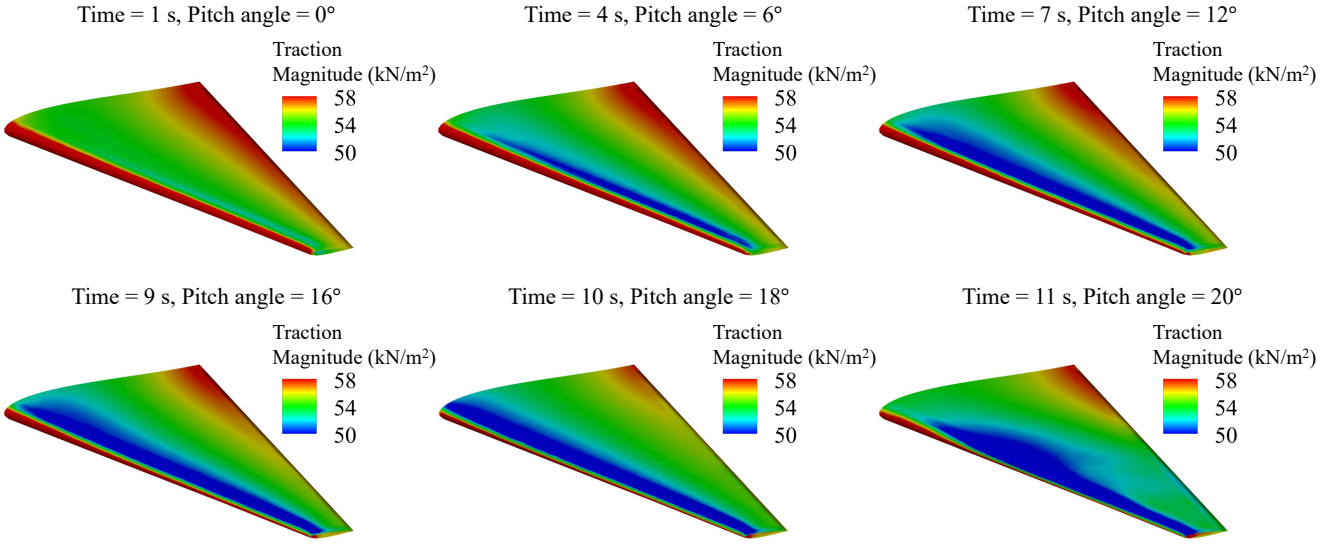

Fig. 9: Contour plot of the fluid traction magnitude acting on the horizontal stabilizer at different time instances.

time instances. The 3D stresses at all the integration points of the continuum shell patch are extracted, and the equivalent von Mises stresses are then calculated to facilitate a simple frequency-domain fatigue damage evaluation. The time histories of the 3D stresses and the corresponding equivalent stress at the location with the highest stress value of the continuum shell patch, which is evaluated in both the in-plane and through-thickness directions, are plotted in Figures 11 and 12, respectively.

A simple frequency-domain fatigue damage analysis is carried out based on the obtained time history of the stresses. Specifically, the Fast Fourier Transform (FFT) technique is employed in the first step to convert the time-domain signals to frequency domain in terms of power spectral densities (PSD) (cf. Figure 13). A number of numerical strategies are adopted during the process to obtain a stable conversion, including mean removal and Hanning window to smoothen abrupt ends and reduce leakage in the resulting Fourier transform. In the next step, Dirlik's probability distribution of stress cycles [69] is computed and a fatigue damage intensity index D at every integration point is cumulatively assessed based on the corresponding S-N look-up

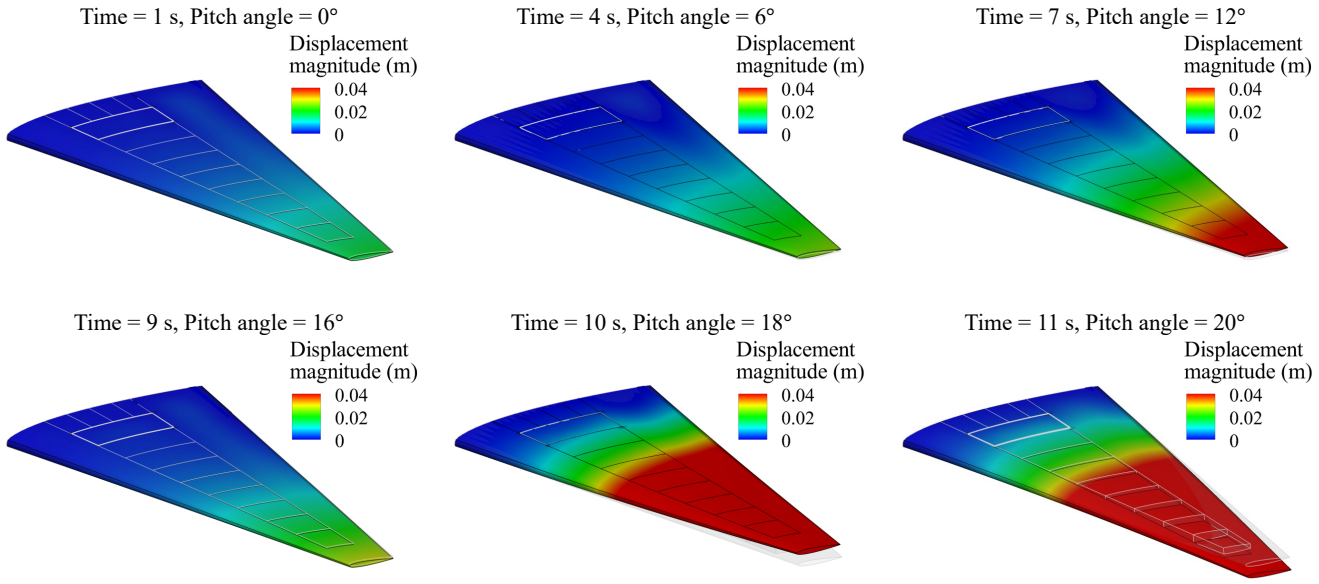

Fig. 10: Displacement magnitude contour of the horizontal stabilizer at different time instances overlapped with the reference configuration (light gray edges). The deformation is scaled up 5 times for visualization.

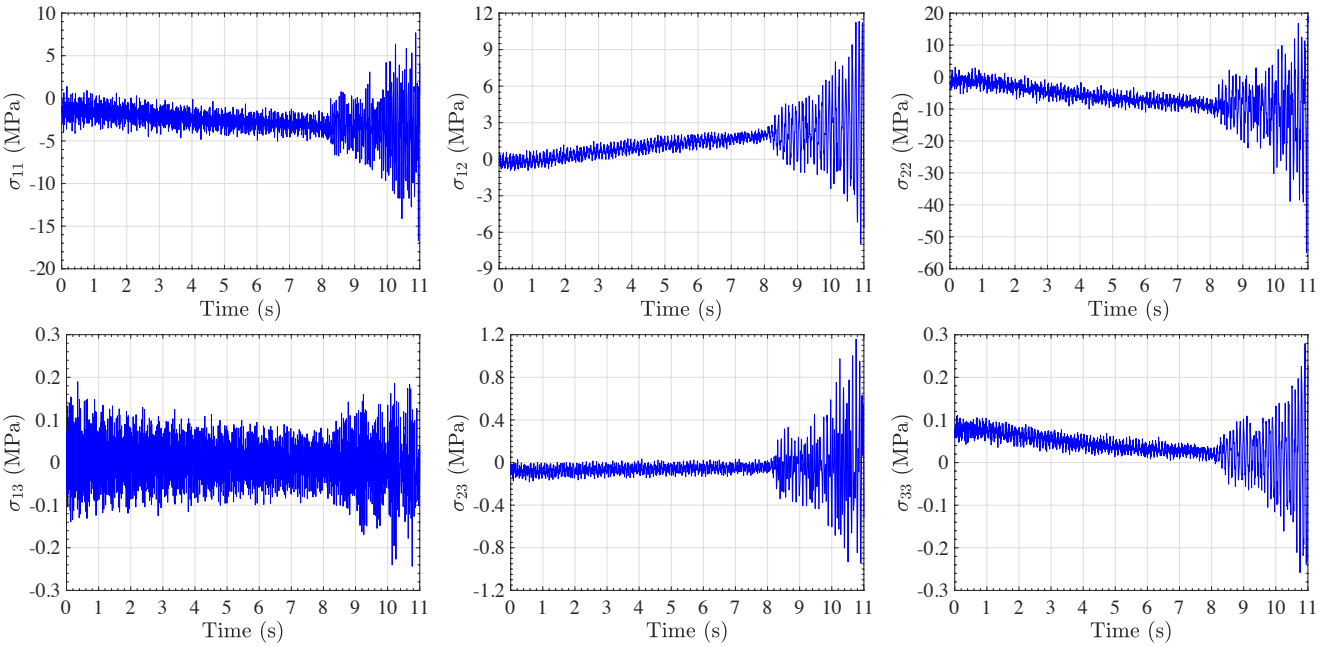

Fig. 11: The 3D Cauchy stress time histories at the location with the highest stress value of the continuum shell patch. Note that the vertical axes are scaled to clearly visualize the data for each stress component.

curves. Dirlik's probabilistic distribution $p(\sigma)$ can be written in the following form,

$$p(\sigma) = \frac{1}{\sqrt{m_0}}\left(\frac{D_1}{Q}e^{-\frac{Z}{Q}} + \frac{D_2 Z}{R^2}e^{-\frac{Z^2}{2R^2}} + \frac{D_3}{Z}e^{-\frac{Z^2}{2}}\right), \tag{15}$$

where

$$D_1 = \frac{2(X_m - \gamma^2)}{1+\gamma^2}, \quad D_2 = \frac{1-\gamma-D_1+D_1^2}{1-R},$$
$$D_3 = 1 - D_1 - D_2, \quad Z = \frac{\sigma}{\sqrt{m_0}},$$

$$Q = \frac{1.25(\gamma - D_3 - D_2 R)}{D_1}, \quad R = \frac{\gamma - X_m - D_1^2}{1-\gamma-D_1+D_1^2},$$
$$X_m = \frac{m_1}{m_0}\sqrt{\frac{m_2}{m_4}}, \quad \gamma = \frac{m_2}{\sqrt{m_0 m_4}}. \tag{16}$$

The spectral moments m_0, m_1, m_2 and m_4 of a signal $G_{xx}(f)$ are given as,

$$m_i = \int_0^\infty f^i G_{xx}(f) df. \tag{17}$$

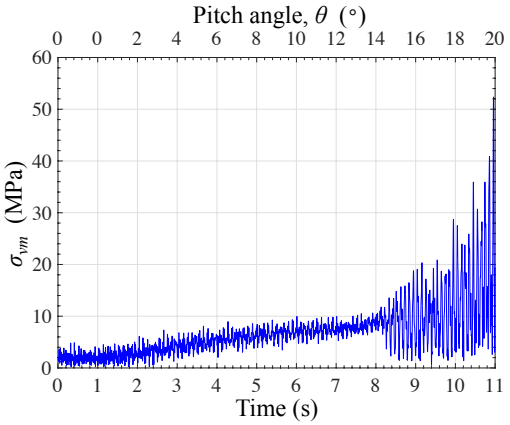

Fig. 12: The computed time history of the von Mises stress at the location with the highest stress value on the stabilizer.

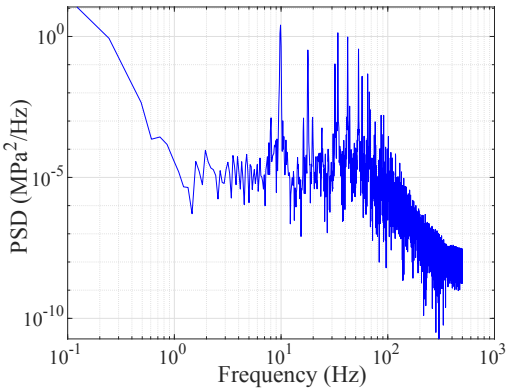

Fig. 13: The response power spectral density (PSD).

The cumulative fatigue damage intensity index D per unit time can be written as,

$$D = \int_0^\infty \frac{\nu_a p(\sigma)}{N_f(\sigma)} d\sigma \,, \tag{18}$$

with ν_a the expected peak occurrence frequency, $\nu_a = \sqrt{\frac{m_4}{m_2}}$, and N_f the corresponding fatigue life. In the current study, a representative S-N curve for general aluminium alloy materials is employed,

$$\sigma_{\mathrm{vm}}^a \cdot N_{\mathrm{f}} = C \,, \tag{19}$$

with a and C being material parameters, $a = 4.10$, $C = 3.15 \times 10^{14}$, and σ_{vm} the equivalent von Mises stress.

Finally, the fatigue life in terms of time can be obtained by taking the reciprocal of D. Using the above approach, the fatigue life at the location with the highest stress value on the continuum shell patch is computed as 3.47×10^5 hrs. Note that the location of the continuum shell patch in this study is not necessarily representative of the most critical location of the stabilizer. A full fatigue evaluation of the entire stabilizer, or at least at critical regions, is needed in order to assess the component-level integrity and identify critical locations. Also note that an idealized stabilizer structure is considered in this work, and as a result, the reported fatigue life may not represent a realistic scenario. The above calculation is intended to demonstrate the complete workflow of the developed computational framework.

4 Conclusion

An isogeometric blended shell approach is developed for efficient prediction of the 3D stresses and buffet-induced fatigue evaluation of aircraft horizontal stabilizers. The key feature of the method is the deployment of continuum shells only at critical locations for accurate 3D stress prediction and the use of KL shells at other non-critical regions to improve computational efficiency. A dynamic nonlinear analysis of a representative aircraft horizontal stabilizer is employed to demonstrate the numerical accuracy and computational efficiency of the developed approach. After that, a hybrid IMGA-BF CFD analysis of flow over the full-scale aircraft is performed to generate realistic aerodynamic loads on the stabilizer external surface for dynamic analysis, and a frequency-domain fatigue analysis is subsequently carried out to assess the buffet-induced fatigue damage and remaining fatigue life. The proposed approach offers the possibility to model high-fidelity structural response and buffet-induced fatigue damage in large-scale aircraft structures within a manageable amount of time.

Acknowledgments

This work is supported by the U.S. Naval Air Systems Command (NAVAIR) under Grant No. N68335-20-C-0899. This support is gratefully acknowledged.

References

1. N. Liu, X. Cui, J. Xiao, J. Lua, and N. Phan. A simplified continuum damage mechanics based modeling strategy for cumulative fatigue damage assessment of metallic bolted joints. *International Journal of Fatigue*, 131:105302, 2020.
2. N. Liu, J. Xiao, X. Cui, P. Liu, and J. Lua. A continuum damage mechanics (CDM) modeling approach for prediction of fatigue failure of metallic bolted joints. In *In AIAA Scitech 2019 Forum*, AIAA 2019-0237, 2019.
3. J. Kiendl, K.-U. Bletzinger, J. Linhard, and R. Wüchner. Isogeometric shell analysis with Kirchhoff–Love elements. *Computer Methods in Applied Mechanics and Engineering*, 198:3902–3914, 2009.
4. J. Kiendl, M.-C. Hsu, M. C. H. Wu, and A. Reali. Isogeometric Kirchhoff–Love shell formulations for general hyperelastic materials. *Computer Methods in Applied Mechanics and Engineering*, 291:280–303, 2015.
5. T. J. R. Hughes, J. A. Cottrell, and Y. Bazilevs. Isogeometric analysis: CAD, finite elements, NURBS, exact geometry, and mesh refinement. *Computer Methods in Applied Mechanics and Engineering*, 194:4135–4195, 2005.

6. N. Liu and A. E. Jeffers. A geometrically exact isogeometric Kirchhoff plate: Feature-preserving automatic meshing and C 1 rational triangular Bézier spline discretizations. *International Journal for Numerical Methods in Engineering*, 115(3):395–409, 2018.
7. A. J. Herrema, J. Kiendl, and M.-C. Hsu. A framework for isogeometric-analysis-based optimization of wind turbine blade structures. *Wind Energy*, 22:153–170, 2019.
8. N. Liu and A. E. Jeffers. Feature-preserving rational Bézier triangles for isogeometric analysis of higher-order gradient damage models. *Computer Methods in Applied Mechanics and Engineering*, 357:112585, 2019.
9. N. Liu and A. E. Jeffers. Rational Bézier triangles for the analysis of isogeometric higher-order gradient damage models. In *13th World Congress on Computational Mechanics (WCCM XIII) and 2nd Pan American Congress on Computational Mechanics (PANACM II), New York City, NY, USA*, 2018.
10. N. Liu. *Non-uniform rational B-splines and rational Bezier triangles for isogeometric analysis of structural applications*. PhD thesis, University of Michigan, 2018.
11. E. L. Johnson and M.-C. Hsu. Isogeometric analysis of ice accretion on wind turbine blades. *Computational Mechanics*, 66:311–322, 2020.
12. E. L. Johnson, D. W. Laurence, F. Xu, C. E. Crisp, A. Mir, H. M. Burkhart, C.-H. Lee, and M.-C. Hsu. Parameterization, geometric modeling, and isogeometric analysis of tricuspid valves. *Computer Methods in Applied Mechanics and Engineering*, 384:113960, 2021.
13. K. Takizawa, T. E. Tezduyar, Y. Otoguro, T. Terahara, T. Kuraishi, and H. Hattori. Turbocharger flow computations with the Space–Time Isogeometric Analysis (ST-IGA). *Computers & Fluids*, 142:15–20, 2017.
14. K. Takizawa, T. E. Tezduyar, and T. Terahara. Ram-air parachute structural and fluid mechanics computations with the space–time isogeometric analysis (ST-IGA). *Computers & Fluids*, 141:191–200, 2016.
15. K. Takizawa, T. E. Tezduyar, and T. Sasaki. Aorta modeling with the element-based zero-stress state and isogeometric discretization. *Computational Mechanics*, 59:265–280, 2017.
16. K. Takizawa, T. E. Tezduyar, T. Terahara, and T. Sasaki. Heart valve flow computation with the integrated Space–Time VMS, Slip Interface, Topology Change and Isogeometric Discretization methods. *Computers & Fluids*, 158:176–188, 2017.
17. N. Liu and A. E. Jeffers. Isogeometric analysis of laminated composite and functionally graded sandwich plates based on a layerwise displacement theory. *Composite Structures*, 176:143–153, 2017.
18. N. Liu and A. E. Jeffers. Adaptive isogeometric analysis in structural frames using a layer-based discretization to model spread of plasticity. *Computers & Structures*, 196:1–11, 2018.
19. N. Liu, P. A. Beata, and A. E. Jeffers. A mixed isogeometric analysis and control volume approach for heat transfer analysis of nonuniformly heated plates. *Numerical Heat Transfer, Part B: Fundamentals*, 75(6):347–362, 2019.
20. D. J. Benson, Y. Bazilevs, M.-C. Hsu, and T. J. R. Hughes. A large deformation, rotation-free, isogeometric shell. *Computer Methods in Applied Mechanics and Engineering*, 200:1367–1378, 2011.
21. K. Takizawa, T. E. Tezduyar, and T. Sasaki. Isogeometric hyperelastic shell analysis with out-of-plane deformation mapping. *Computational Mechanics*, 63:681–700, 2019.
22. N. Liu, X. Ren, and J. Lua. An isogeometric continuum shell element for modeling the nonlinear response of functionally graded material structures. *Composite Structures*, 237:111893, 2020.
23. N. Liu, M.-C. Hsu, J. Lua, and N. Phan. A large deformation isogeometric continuum shell formulation incorporating finite strain elastoplasticity. *Computational Mechanics*, Accepted, 2022. https://doi.org/10.1007/s00466-022-02193-8.
24. S. Hosseini, J. J. C. Remmers, C. V. Verhoosel, and R. De Borst. An isogeometric continuum shell element for non-linear analysis. *Computer Methods in Applied Mechanics and Engineering*, 271:1–22, 2014.
25. Y. Guo and M. Ruess. A layerwise isogeometric approach for nurbs-derived laminate composite shells. *Composite Structures*, 124:300–309, 2015.
26. L. Leonetti, F. Liguori, D. Magisano, and G. Garcea. An efficient isogeometric solid-shell formulation for geometrically nonlinear analysis of elastic shells. *Computer Methods in Applied Mechanics and Engineering*, 331:159–183, 2018.
27. A. J. Herrema, E. L. Johnson, D. Proserpio, M. C. H. Wu, J. Kiendl, and M.-C. Hsu. Penalty coupling of non-matching isogeometric Kirchhoff–Love shell patches with application to composite wind turbine blades. *Computer Methods in Applied Mechanics and Engineering*, 346:810–840, 2019.
28. J. Kiendl, Y. Bazilevs, M.-C. Hsu, R. Wüchner, and K.-U. Bletzinger. The bending strip method for isogeometric analysis of Kirchhoff–Love shell structures comprised of multiple patches. *Computer Methods in Applied Mechanics and Engineering*, 199:2403–2416, 2010.
29. A. Goyal and B. Simeon. On penalty-free formulations for multi-patch isogeometric kirchhoff–love shells. *Mathematics and Computers in Simulation*, 136:78–103, 2017.
30. L. Leonetti, F. S. Liguori, D. Magisano, J. Kiendl, A. Reali, and G. Garcea. A robust penalty coupling of non-matching isogeometric kirchhoff–love shell patches in large deformations. *Computer Methods in Applied Mechanics and Engineering*, 371:113289, 2020.
31. N. Liu, E. L. Johnson, M. R. Rajanna, J. Lua, N. Phan, and M.-C. Hsu. Blended isogeometric Kirchhoff–Love and continuum shells. *Computer Methods in Applied Mechanics and Engineering*, 385:114005, 2021.
32. N. Liu, J. Lua, M. R. Rajanna, E. L. Johnson, M.-C. Hsu, and N. D. Phan. Buffet-induced structural response prediction of aircraft horizontal stabilizers based on immersogeometric analysis and an isogeometric blended shell approach. In *AIAA SCITECH 2022 Forum*, page 0852, 2022.
33. Y. Bazilevs, M.-C. Hsu, J. Kiendl, R. Wüchner, and K.-U. Bletzinger. 3D simulation of wind turbine rotors at full scale. Part II: Fluid–structure interaction modeling with composite blades. *International Journal for Numerical Methods in Fluids*, 65:236–253, 2011.
34. Y. Bazilevs, M.-C. Hsu, and M. A. Scott. Isogeometric fluid–structure interaction analysis with emphasis on non-matching discretizations, and with application to wind turbines. *Computer Methods in Applied Mechanics and Engineering*, 249–252:28–41, 2012.
35. M.-C. Hsu and Y. Bazilevs. Fluid–structure interaction modeling of wind turbines: simulating the full machine. *Computational Mechanics*, 50:821–833, 2012.
36. A. Korobenko, M.-C. Hsu, I. Akkerman, J. Tippmann, and Y. Bazilevs. Structural mechanics modeling and FSI simulation of wind turbines. *Mathematical Models and Methods in Applied Sciences*, 23(2):249–272, 2013.
37. Y. Bazilevs, A. Korobenko, X. Deng, and J. Yan. Novel structural modeling and mesh moving techniques for advanced fluid–structure interaction simulation of wind turbines. *International Journal for Numerical Methods in Engineering*, 102(3-4):766–783, 2014.
38. J. Yan, A. Korobenko, X. Deng, and Y. Bazilevs. Computational free-surface fluid–structure interaction with application to floating offshore wind turbines. *Computers & Fluids*, 141:155–174, 2016.

39. A. Korobenko, J. Yan, S. M. I. Gohari, S. Sarkar, and Y. Bazilevs. FSI simulation of two back-to-back wind turbines in atmospheric boundary layer flow. *Computers & Fluids*, 158:167–175, 2017.
40. Y. Bazilevs, J. Yan, X. Deng, and A. Korobenko. Computer modeling of wind turbines: 2. Free-surface FSI and fatigue-damage. *Archives of Computational Methods in Engineering*, 26:1101–1115, 2018.
41. M.-C. Hsu, D. Kamensky, Y. Bazilevs, M. S. Sacks, and T. J. R. Hughes. Fluid–structure interaction analysis of bioprosthetic heart valves: significance of arterial wall deformation. *Computational Mechanics*, 54(4):1055–1071, 2014.
42. D. Kamensky, M.-C. Hsu, D. Schillinger, J. A. Evans, A. Aggarwal, Y. Bazilevs, M. S. Sacks, and T. J. R. Hughes. An immersogeometric variational framework for fluid–structure interaction: Application to bioprosthetic heart valves. *Computer Methods in Applied Mechanics and Engineering*, 284:1005–1053, 2015.
43. M.-C. Hsu, D. Kamensky, F. Xu, J. Kiendl, C. Wang, M. C. H. Wu, J. Mineroff, A. Reali, Y. Bazilevs, and M. S. Sacks. Dynamic and fluid–structure interaction simulations of bioprosthetic heart valves using parametric design with T-splines and Fung–type material models. *Computational Mechanics*, 55:1211–1225, 2015.
44. F. Xu, S. Morganti, R. Zakerzadeh, D. Kamensky, F. Auricchio, A. Reali, T. J. R. Hughes, M. S. Sacks, and M.-C. Hsu. A framework for designing patient-specific bioprosthetic heart valves using immersogeometric fluid–structure interaction analysis. *International Journal for Numerical Methods in Biomedical Engineering*, 34:e2938, 2018.
45. M. C. H. Wu, R. Zakerzadeh, D. Kamensky, J. Kiendl, M. S. Sacks, and M.-C. Hsu. An anisotropic constitutive model for immersogeometric fluid–structure interaction analysis of bioprosthetic heart valves. *Journal of Biomechanics*, 74:23–31, 2018.
46. A. Balu, S. Nallagonda, F. Xu, A. Krishnamurthy, M.-C. Hsu, and S. Sarkar. A deep learning framework for design and analysis of surgical bioprosthetic heart valves. *Scientific Reports*, 9:18560, 2019.
47. F. Xu, E. L. Johnson, C. Wang, A. Jafari, C.-H. Yang, M. S. Sacks, A. Krishnamurthy, and M.-C. Hsu. Computational investigation of left ventricular hemodynamics following bioprosthetic aortic and mitral valve replacement. *Mechanics Research Communications*, 112:103604, 2021.
48. D. Kamensky. Open-source immersogeometric analysis of fluid–structure interaction using FEniCS and tIGAr. *Computers and Mathematics with Applications*, 81:634–648, 2021.
49. F. Xu, Y. Bazilevs, and M.-C. Hsu. Immersogeometric analysis of compressible flows with application to aerodynamic simulation of rotorcraft. *Mathematical Models and Methods in Applied Sciences*, 29:905–938, 2019.
50. T. E. Tezduyar, S. K. Aliabadi, M. Behr, and S. Mittal. Massively parallel finite element simulation of compressible and incompressible flows. *Computer Methods in Applied Mechanics and Engineering*, 119:157–177, 1994.
51. T. Tezduyar, S. Aliabadi, M. Behr, A. Johnson, V. Kalro, and M. Litke. Flow simulation and high performance computing. *Computational Mechanics*, 18:397–412, 1996.
52. F. Xu, D. Schillinger, D. Kamensky, V. Varduhn, C. Wang, and M.-C. Hsu. The tetrahedral finite cell method for fluids: Immersogeometric analysis of turbulent flow around complex geometries. *Computers & Fluids*, 141:135–154, 2016.
53. M.-C. Hsu, C. Wang, F. Xu, A. J. Herrema, and A. Krishnamurthy. Direct immersogeometric fluid flow analysis using B-rep CAD models. *Computer Aided Geometric Design*, 43:143–158, 2016.
54. C. Wang, F. Xu, M.-C. Hsu, and A. Krishnamurthy. Rapid B-rep model preprocessing for immersogeometric analysis using analytic surfaces. *Computer Aided Geometric Design*, 52-53:190–204, 2017.
55. Q. Zhu, F. Xu, S. Xu, M.-C. Hsu, and J. Yan. An immersogeometric formulation for free-surface flows with application to marine engineering problems. *Computer Methods in Applied Mechanics and Engineering*, 361:112748, 2020.
56. K. Saurabh, B. Gao, M. Fernando, S. Xu, M. A. Khanwale, B. Khara, M.-C. Hsu, A. Krishnamurthy, H. Sundar, and B. Ganapathysubramanian. Industrial scale Large Eddy Simulations with adaptive octree meshes using immersogeometric analysis. *Computers & Mathematics with Applications*, 97:28–44, 2021.
57. A. Preumont. *Random Vibration and Spectral Analysis/Vibrations aléatoires et analyse spectral*, volume 33. Springer Science & Business Media, 1994.
58. J. Chung and G. M. Hulbert. A time integration algorithm for structural dynamics with improved numerical dissipation: The generalized-α method. *Journal of Applied Mechanics*, 60:371–75, 1993.
59. K. E. Jansen, C. H. Whiting, and G. M. Hulbert. A generalized-α method for integrating the filtered Navier-Stokes equations with a stabilized finite element method. *Computer Methods in Applied Mechanics and Engineering*, 190:305–319, 2000.
60. Y. Bazilevs, V. M. Calo, T. J. R. Hughes, and Y. Zhang. Isogeometric fluid–structure interaction: theory, algorithms, and computations. *Computational Mechanics*, 43:3–37, 2008.
61. F. Xu, G. Moutsanidis, D. Kamensky, M.-C. Hsu, M. Murugan, A. Ghoshal, and Y. Bazilevs. Compressible flows on moving domains: Stabilized methods, weakly enforced essential boundary conditions, sliding interfaces, and application to gas-turbine modeling. *Computers & Fluids*, 158:201–220, 2017.
62. N. Kozak, F. Xu, M. R. Rajanna, L. Bravo, M. Murugan, A. Ghoshal, Y. Bazilevs, and M.-C. Hsu. High-fidelity finite element modeling and analysis of adaptive gas turbine stator-rotor flow interaction at off-design conditions. *Journal of Mechanics*, 36:595–606, 2020.
63. Y. Bazilevs, K. Takizawa, M. C. H. Wu, T. Kuraishi, R. Avsar, Z. Xu, and T. E. Tezduyar. Gas turbine computational flow and structure analysis with isogeometric discretization and a complex-geometry mesh generation method. *Computational Mechanics*, 67:57–84, 2021.
64. D. Codoni, G. Moutsanidis, M.-C. Hsu, Y. Bazilevs, C. Johansen, and A. Korobenko. Stabilized methods for high-speed compressible flows: toward hypersonic simulations. *Computational Mechanics*, 67:785–809, 2021.
65. M. R. Rajanna, E. L. Johnson, D. Codoni, A. Korobenko, Y. Bazilevs, N. Liu, J. Lua, N. D. Phan, and M.-C. Hsu. Finite element methodology for modeling aircraft aerodynamics: development, simulation, and validation. *Computational Mechanics*, Accepted, 2022. https://doi.org/10.1007/s00466-022-02178-7.
66. M. R. Rajanna, E. L. Johnson, D. Codoni, A. Korobenko, Y. Bazilevs, N. Liu, J. Lua, N. D. Phan, and M.-C. Hsu. Finite element simulation and validation for aerospace applications: Stabilized methods, weak dirichlet boundary conditions, and discontinuity capturing for compressible flows. In *AIAA SCITECH 2022 Forum*, page 1077, 2022.
67. T. E. Tezduyar, K. Takizawa, C. Moorman, S. Wright, and J. Christopher. Space–time finite element computation of complex fluid–structure interactions. *International Journal for Numerical Methods in Fluids*, 64:1201–1218, 2010.
68. T. E. Tezduyar. Finite element methods for flow problems with moving boundaries and interfaces. *Archives of Computational Methods in Engineering*, 8:83–130, 2001.
69. X. Pitoiset and A. Preumont. Spectral methods for multiaxial random fatigue analysis of metallic structures. *International Journal of Fatigue*, 22(7):541–550, 2000.